PAPER

Layer breathing and shear modes in multilayer graphene: a DFT-vdW study

IOP Publishing Journal of Physics: Condensed Matter
J. Phys.: Condens. Matter **31** (2019) 295301 (8pp) https://doi.org/10.1088/1361-648X/ab1995

Layer breathing and shear modes in multilayer graphene: a DFT-vdW study

Rafael R Del Grande, Marcos G Menezes and Rodrigo B Capaz

Instituto de Física, Universidade Federal do Rio de Janeiro, Caixa Postal 68528, Rio de Janeiro, RJ 21941-972, Brazil

E-mail: rdgrande@if.ufrj.br, marcosgm@if.ufrj.br and capaz@if.ufrj.br

Received 21 February 2019, revised 8 April 2019
Accepted for publication 15 April 2019
Published 8 May 2019

Abstract

In this work, we study structural and vibrational properties of multilayer graphene using density-functional theory with van der Waals (vdW) functionals. Initially, we analyze how different vdW functionals compare by evaluating the lattice parameters, elastic constants and vibrational frequencies of low energy optical modes of graphite. Our results indicate that the vdW-DF1-optB88 functional has the best overall performance on the description of vibrational properties. Next, we use this functional to study the influence of the vdW interactions on the structural and vibrational properties of multilayer graphene. Specifically, we evaluate binding energies, interlayer distances and phonon frequencies of layer breathing and shear modes. We observe excellent agreement between our calculated results and available experimental data, which suggests that this functional has truly predictive power for layer-breathing and shear frequencies that have not been measured yet. This indicates that careful selected vdW functionals can describe interlayer bonding in graphene-related systems with good accuracy.

Keywords: graphene, multilayer graphene, van der Waals, DFT, layer breathing mode, shear mode

(Some figures may appear in colour only in the online journal)

1. Introduction

Since the experimental realization of graphene [1–5], an extensive number of studies have been made on this material and related structures due to their remarkable properties and potential applications [6–10]. In particular, one class of graphene related materials that is of great interest is multilayer graphene. *N*-layer graphene (NLG) consists of *N* stacked graphene layers, which can have different orientations with respect to each other. Their mechanical, electronic and optical properties strongly depend on *N* and their relative [11, 12] orientations, resulting in a wide variety of potential applications [13, 14].

These materials are stable due to the van der Waals (vdW) interactions between layers (as in graphite). Therefore, in order to study them from a theoretical point of view, one needs a good description of these dispersive interactions, specially for properties related to interlayer bonding, stiffness and vibrations. In particular, the effects of vdW interactions can be detected in Raman spectroscopy, as interlayer vibrations in 2D materials can be measured by this technique with great precision. For this reason, Raman scattering may be used as a tool to evaluate the accuracy of various theoretical implementations of vdW interactions in density-functional theory (DFT) calculations [15–21].

In DFT, the exact exchange-correlation functional should in principle contain vdW interactions. However, the exact functional is unknown, and commonly used local (LDA) and semilocal (GGA) approximations do not capture the effects of vdW interactions, which are dispersion forces arising from long-range electron-electron correlations [22, 23]. In graphite, it is known that GGA functionals considerably overestimate the interlayer distance, while describing well the in-plane carbon–carbon distances. On the other hand, LDA functionals give a good interplanar distance (although smaller than the experimental value) and underestimates the covalent bond lengths [24].

Table 1. Calculated lattice parameters a_0 and c_0, elastic constants, C_{13}, C_{33} and $C_{11}+C_{12}$, binding energies ΔE_b, frequencies of shear and LBM of graphite and mean relative dispersion Δ and Δ_{freq} (explained in text), as given by different functionals employed on this work.

	a_0 (Å)	c_0 (Å)	C_{13} (GPa)	C_{33} (GPa)	$C_{11}+C_{12}$ (GPa)	ΔE_b (J m^{-2})	Shear mode (cm^{-1})	LBM (cm^{-1})	Δ (%)	Δ_{freq} (%)
Exp. values	2.459[b]	6.706[b]	15[c] 0[d]	36.5[c] 38.7[d]	1240[c] 1248[d]	0.32 ± 0.03[g], 0.19 ± 0.01[h] 0.21 ± 0.06[i], 0.33[j]	42[e] 43.5[f], 44.03[k]	127[e]	—	—
Reference values[a]	—	6.706	—	37.6	—	0.2625	43.2	127	—	—
This work										
GGA	2.46	8.27	−0.5	3.7	1005.9	0.01	10.4	36.7	71.4	73.5
LDA	2.45	6.62	−2.8	32.0	1309.5	0.15	44.2	118.8	13.6	4.4
RVV10	2.48	6.71	−4.3	44.7	1210.3	0.43	42.4	145.0	19.7	8.0
vdW-DF1	2.47	7.15	−2.8	27.1	1124.9	0.33	28.2	108.7	21.9	24.5
vdW-DF1-c09	2.46	6.45	−4.0	48.2	1299.4	0.47	50.9	151.5	29.7	18.6
vdw-DF1-cx	2.46	6.55	−3.8	47.7	1276.9	0.40	47.1	137.5	19.8	8.7
vdW-DF1-optB86b	2.46	6.61	−3.9	48.1	1255.3	0.44	44.8	138.9	22.0	6.6
vdW-DF1-optB88	2.47	6.68	−3.7	42.2	1230.2	0.43	42.2	138.6	17.6	5.7
vdW-DF2	2.49	7.05	−3.3	34.7	1111.1	0.33	31.9	123.4	13.5	14.5
vdW-DF2-B86r	2.47	6.63	−4.0	40.7	1250.1	0.37	44.6	137.6	12.4	5.8
vdW-DF2-c09	2.46	6.53	−4.1	42.0	1277.6	0.34	54.3	141.9	16.3	18.8
Other theoretical works										
GGA [24]	2.46	8.49	−0.46	2.4	976	—	8	28	—	—
LDA [24]	2.44	6.68	−2.8	29	1283	—	44	113	—	—
PBE+D2 [41]	2.461	6.444	—	22.04	—	0.34	—	—	—	—
PBE+D3 [41]	2.464	6.965	—	13.09	—	0.29	—	—	—	—
PBE+D3-BJ [41]	2.464	6.745	—	17.16	—	0.32	—	—	—	—
PBE+TS [41]	2.458	6.665	—	34.61	—	0.50	—	—	—	—
PBE+TS+SCS [41]	2.461	6.633	—	26.79	—	0.33	—	—	—	—
ACFDT-RPA [42]	—	6.68	—	36	—	0.29	—	—	—	—
QMC [43]	—	6.852	—	—	—	0.34 ± 0.03	—	—	—	—
LDA [44]	—	6.668	—	23.67	—	0.14	—	—	—	—
LDA+D2 [44]	—	5.978	—	95.23	—	0.70	—	—	—	—
PBE [44]	—	8.838	—	1.390	—	0.005	—	—	—	—
PBE+D2 [44]	—	6.462	—	42.44	—	0.37	—	—	—	—
optPBE+D2 [44]	—	6.894	—	33.15	—	0.39	—	—	—	—
vdW-DF1-optB88 [44]	—	6.712	—	40.37	—	0.42	—	—	—	—
rPW86/vdW-DF2 [44]	—	7.048	—	34.11	—	0.32	—	—	—	—

[a] Mean of experimental values. These values were used as reference values to evaluate the performance of the vdW functionals.
[b] Hanfland *et al* [42].
[c] [43].
[d] Bosak *et al* [44].
[e] Holden *et al* [15].
[f] Tan *et al* [16].
[g] Zacharia *et al* [45].
[h] Liu *et al* [46].
[i] Benedict *et al* [47].
[j] Wang *et al* [48].
[k] Boschetto *et al* [20].

In recent works, non-local vdW exchange-correlation functionals were developed aiming to describe the properties of layered materials, adsorption processes and other phenomena [25–33]. In particular, in the vdW-DF family of functionals [25], the exchange-correlation energy is given by:

$$E_{xc}[n] = E_x^{\text{GGA}}[n] + E_c^{\text{LDA}}[n] + E_c^{\text{nl}}[n] \quad (1)$$

where x and c label the exchange and correlation parts of the corresponding functionals, respectively, and $E_c^{\text{nl}}[n]$ is a non-local correlation energy given by

$$E_c^{\text{nl}}[n] = \int \mathrm{d}^3 r \mathrm{d}^3 r' n(\mathbf{r}) \phi[n](\mathbf{r}, \mathbf{r}') n(\mathbf{r}') \quad (2)$$

where $\phi[n]$ is a two-point kernel function and $n(\mathbf{r})$ is the electronic density. The different functionals in this family consist of different combinations of flavors for the GGA exchange and LDA correlation, as well as different forms for the two-point kernel [25–33]. They were tailored to describe properties of specific systems, such as the interaction energy of dimer pairs and the structure of small molecules. Therefore, their

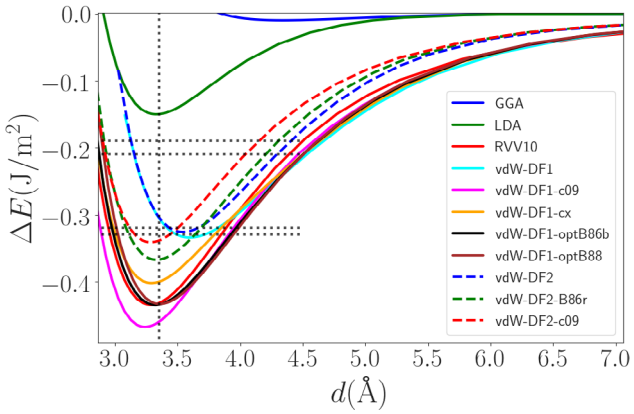

Figure 1. Total energy difference per unit area between graphite and graphene as a function of the interlayer distance for different functionals. The vertical dotted line corresponds to the experimental interlayer distance and horizontal dotted lines correspond to the experimental values reported in table 1. The zero energy corresponds to graphene energy per unit area.

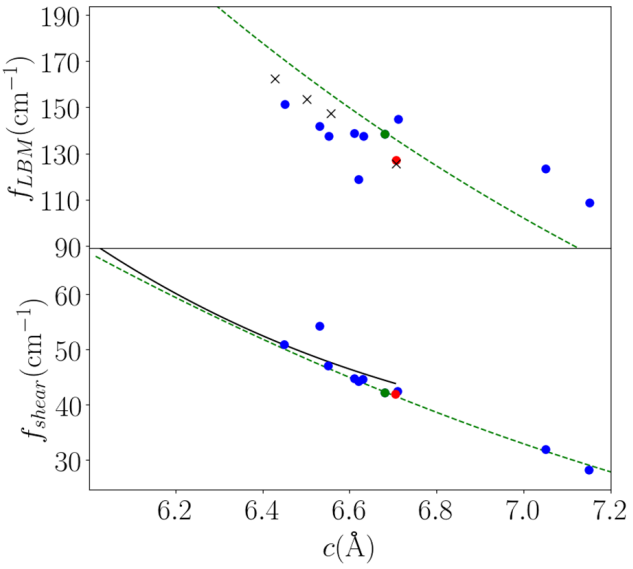

Figure 2. Calculated frequencies for the LBM and shear mode of graphite as a function of the equilibrium out-of-plane lattice constant for each functional used in this work. The data points are taken from table 1 and are represented by green and blue points. The green points are results given by the vdW-DF1-optB88 functional, while blue points are results from other functionals (GGA not included). The green dashed lines correspond to frequencies calculated using the vdW-DF1-optB88 functional for different interlayer distances, which do not correspond to the equilibrium value for this functional. Red points are experimental values from [15]. The black line and black crosses are experimental results from [42] and [54], respectively.

performances can dramatically change depending on chemical environment. For a complete overview see [22] and [34].

In this work, we compare the performances of different vdW functionals from the DF family in describing the elastic constants, binding energy and vibrational frequencies of the shear and layer breathing modes (LBM) of graphite. Our results indicate that the vdW-DF1-optB88 functional is the best suited functional for graphene-based systems. Next, we use this functional to calculate interlayer distances, binding energies and phonon frequencies of NLG. We find that the inclusion of vdW interactions is especially important for an accurate description of interlayer distances and out-of-plane vibrational modes.

2. Methods

All DFT calculations were performed using the quantum espresso package [34, 35]. Energy cutoffs of 60 and 480 Ry are used for the plane-wave expansion of the wavefunctions and electronic density, respectively. For graphite calculations, several functionals are used. For LDA and GGA calculations, we use the PZ and PBE functionals, respectively [36, 37]. For vdW calculations, we employ different functionals from the vdW-DF family [25–33]. In all cases, we use Rappe–Rabe–Kaxiras–Joannopoulos (RRKJ) ultrasoft pseudopotentials for the ion–electron interaction, including a non-linear core correction [38]. It should be noted that, so far, pseudopotentials for non-local functionals have not been developed, so we use a GGA-derived potential for the vdW calculations as in [32].

Structural optimizations are done with a convergence threshold on forces of 10^{-6} Ry Bohr^{-1} and on energies of 10^{-5} Ry. To sample the Brillouin Zone, we have used Monkhorst-Pack meshes of dimensions $16 \times 16 \times 16$ for graphite and $16 \times 16 \times 1$ for NLG.

The elastic constants of graphite are calculated from second order derivatives of the total energy with respect to the lattice parameters [24, 39]:

$$\begin{aligned} C_{11} + C_{12} &= \frac{1}{\sqrt{3}c_0}\frac{\partial^2 E}{\partial a^2} \\ C_{33} &= \frac{2c_0}{\sqrt{3}a_0^2}\frac{\partial^2 E}{\partial c^2} \\ C_{13} &= \frac{1}{\sqrt{3}a_0}\frac{\partial^2 E}{\partial a \partial c} \end{aligned} \tag{3}$$

where the derivatives are evaluated at equilibrium. In order to calculate these derivatives, we compute the total energy for several values of a and c around the equilibrium values a_0 and c_0. The resulting energy landscape is then fitted to two-dimensional (2D) fourth order Taylor expansion and the second order coeficients provide the required derivatives. Exfoliation energies per area for graphite and NLG are calculated using the following equation

$$\Delta E_{\mathrm{ex}}(N) = -\frac{(E_N - E_{N-1} - E_{\mathrm{graphene}})}{A} \tag{4}$$

and binding energies per area per layer are calculated using the following equation

$$\Delta E_{\mathrm{b}}(N) = -\frac{(E_N/N - E_{\mathrm{graphene}})}{A} \tag{5}$$

where E_N is the total energy per unit cell of NLG or graphite, and E_{graphene} is the graphene total energy per unit cell, and A is the basal area of the unit cell. All energies are calculated for fully relaxed systems, therefore the calculated exfoliation

energies for NLG include surface relaxation effects. In the case of graphite, in the limit $N \to \infty$, the exfoliation energy coincides with the binding energy [40].

3. Results and discussion

3.1. Graphite

Results for lattice constants, elastic constants, binding energies and vibrational frequencies of graphite are shown in table 1 for different functionals. Note that LDA underestimates the value of a_0 and GGA overestimates the value of c_0, as expected. All vdW functionals give good values of a_0, with the vdw-DF2 showing the largest deviation from the experimental value. For c_0, most vdW functionals show good agreement with experiment. Exceptions are the vdW-DF1 and vdW-DF2 functionals, which show the largest deviations.

All calculated C_{13} values are negative, in agreement with previous theoretical works [24]. Experimental values lie in the range 0–15 GPa, with an error bar of 3 GPa, so a negative value cannot be entirely discarded. Note that most vdW functionals give elastic constants with absolute values larger than LDA as these elastic constants are related to the interactions between graphene layers. Finally, GGA, vdW-DF1 and vdW-DF2 provide inaccurate descriptions of $C_{11} + C_{12}$ because these functionals do not describe very well the interplanar distance. The use of experimental values a_0 and c_0 in equation (3) may improve the evaluation of these elastic constants, as discussed in [24].

In figure 1, the total energy difference (per area and per layer) between graphite and graphene as a function of interlayer separation is shown. The minimum value is, by definition, the negative of the binding energy, whose values for different functionals are also reported in table 1. Experimental values for the exfoliation (or binding) energies are displayed by horizontal dotted lines. We can see that the LDA and GGA functionals give very small values for this quantity in comparison with experimental results while all vdW functionals tend to overestimate it. Our results show a good agreement with other theoretical calculations (reported in table 1) using Quantum Monte Carlo [51], adiabatic-connection fluctuation-dissipation theorem in the random phase approximation (ACFDT-RPA) [50], DFT-D and TS-vdW methods [49, 52] and vdW functionals [52]. For vdW functionals, it is possible to see two families of curves in the range from 4 Å to 7 Å. The solid lines are the vdW-DF type functionals and dashed lines are vdW-DF2 type functionals. Each set converges to a particular asymptotic curve, due to the different asymptotic behaviors of DF1 and DF2 kernels in equation (2) [27].

By using the frozen-phonon technique, the frequencies of the shear and LBM are calculated and reported in table 1. In this technique, phonon frequencies are calculated from the curvature of the energy versus displacement curves. The atomic displacements are performed according to a given normal mode, such that the energy differences with respect to the equilibrium configuration are solely due to this mode [53]. Several vdW functionals (and, interestingly, also LDA) display frequencies with reasonably good agreement with experiment [15, 16].

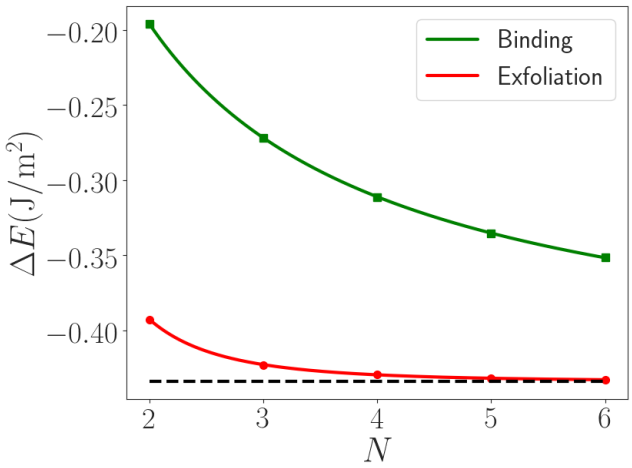

Figure 3. Binding (green square dots) and exfoliation (red circular dots) energies per unit area of NLG as a function of the number of layers using vdW-DF1-optB88 functional. The dashed line corresponds to graphite binding energy and solid lines are fits given by equation (6).

To evaluate the performance of different functionals we calculated the mean relative standard deviation $\Delta = (\sum_i \sqrt{(x_{\mathrm{calc},i} - x_{\mathrm{ref},i})^2}/x_{\mathrm{ref},i})/M$ (M is the number of evaluated properties) between calculated and reference experimental values ($x_{\mathrm{ref},i}$) for each functional using the following quantities: c_0, C_{33}, ΔE_{b} and the frequencies of shear and LBM, as these quantities strongly depend on vdW interactions. C_{13} was not taken into account as all calculated values are far from experimental values reported in table 1. The reference experimental values are taken as the mean of avaiable experimental data and they are also shown in table 1. Based on this analysis, the functional with best overall performance would be vdW-DF2-B86r. However, since our main objective in this work is the calculation of vibrational frequencies in NLG, we also calculate the mean deviation restricted to the LBM and shear-mode vibrational frequencies, labeled Δ_{freq} in table 1. Based on this more restricted analysis the vdW-DF1-optB88 functional shows the best performance with a standard deviation of 5.7%. It should also be mentioned that, even though the LDA functional also has a good performance, it gives a quite poor description of the binding energy of graphite, so we choose the vdW-DF1-optB88 for the study of the vibrational properties of NLG.

By analizing the results in table 1, we notice a correlation, shown in figure 2, between equilibrium c lattice parameters and calculated frequencies using different functionals (green and blue circles). Frequencies tend to be higher for smaller interlayer distances. As a matter of fact, this seems to be a fairly universal trend, as it is approximately followed by experimental results in graphite at zero (red circles) and non-zero pressures (black line and crosses), and also by calculations

Table 2. Interlayer distance and energy difference between AA and AB stackings ($E_{AA} - E_{AB}$) for graphite and 2LG.

		Interlayer distance (Å)		
		AA	AB	$E_{AA} - E_{AB}$ (meV/atom)
Graphite	vdW-DF1-optB88	3.528	3.343	10.5
	vdW-DF1-optB86b	3.522	3.316	11.3
2LG	vdW-DF1-optB88	3.462	3.362	4.7
	vdW-DF1-optB86b	3.522	3.316	5.0
	Exp [55]	—	3.35	—

using the vdW-DF1-optB88 functional and varying the interplanar distance (green dashed line). As one can see, the results for this functional follow very well the experimental trends as a function of pressure.

3.2. N-layer graphene

By using the vdW-DF1-optB88 functional, we evaluated the structural and vibrational properties of multilayer graphene, from the bilayer ($N = 2$) up to six stacked layers. In all cases, the layers are AB (Bernal) stacked. The calculated binding and exfoliation energies are shown in figure 3. As expected, they both converge to the graphite value with increasing number of layers. The green and red curves are fits given by the following equation:

$$\Delta E_{ex(b)}(N) = \frac{A}{N^b} + \Delta E_{ex(b)}(\infty) \tag{6}$$

where $\Delta E_{ex(b)}(\infty)$ corresponds to graphite. For NLG, by using the vdW-DF1-optB88 functional, we find $b = 0.90$ for the binding case and $b = 3.20$ for the exfoliation case. Therefore, the binding energy varies more slowly with N, but both binding and exfoliation energies yield the graphite exfoliation energy $\Delta E_{ex}(\infty)$ in the limit $N \to \infty$, as expected. In fact, the values of $\Delta E_{ex}(\infty)$ as given by each fit differ from the actual value by less than 0.014 J m^{-2}. We have also calculated the interlayer distances in all cases and variations with respect to graphite values are smaller than 0.015 Å.

We also evaluated the interlayer distance and the energy difference between AA and AB stackings for 2LG and graphite (table 2) due to the increasing importance of studies in twisted bilayer graphene (t2LG) [13]. As t2LG is composed by AA and AB domains the interlayer distance an coupling strength between the layers varies through this material [19].

Phonon frequencies are evaluated by using the method of finite differences. Starting from the relaxed structure in each case, displacements of the ith sheet and in the μ direction ($\mu = x$, y or z) are applied and the forces on the jth sheet and ν direction ($\nu = x$, y or z) are computed. In this work, the evaluated optical modes correspond to rigid displacements of the graphene sheets without any internal displacements. Therefore, the corresponding frequencies are evaluated at the Γ point of the Brillouin Zone, and they are shown in figure 4. Red dots are calculations using vdW-DF1-optb88 functional within the harmonic approximation. Anharmonicity effects are also taken into account by using first-order perturbation theory (see below) and the corresponding results are represented by black triangles. The remaining dots are experimental results (details are given in the figure caption). Wherever experimental results are avaiable, the agreement between theory and experiment is quite good. Therefore, it is safe to assume that our theoretical results have good predictive power for the remaining cases.

The dashed lines in figure 4 are obtained by using a model of interactions of equal magnitude between nearest-neighbor layers in which our system is modeled as N masses connected by $N - 1$ springs to compute the frequencies of the LBM and shear modes. In this model, the frequencies are given by [16, 20]

$$\omega_{N,i}^2 = \frac{\omega_{graphite}^2}{2}\left[1 - \cos\left(\frac{\pi(i-1)}{N}\right)\right], \tag{7}$$

where $i = 2, ..., N$ is the mode index, N is the number of layers and $\omega_{graphite}$ is the frequency of the corresponding mode in graphite. This equation can be used to predict the frequencies of NLG from the corresponding graphite frequencies, as shown by the dashed lines in figure 4. By using the average of available experimental data for graphite frequencies, we have plotted, for clarity, only the curves corresponding to the upper and lower branches of equation (7) ($i = N$ and $i = 2$, respectively) [16, 17, 20]. For both modes, this simple analytical model shows good agreement with our calculated results and available experimental data. This suggest that it is a good approximation to consider only interactions between nearest-neighbor layers. Indeed, as a by-product of our finite-difference phonon calculations, we obtain the effective force constants between pairs of layers for both normal (LBM) and tangential (shear) displacements. They are shown in figure 5 and one can notice that, for all systems, the effective force constants between nearest-neighbor layers is typically one order of magnitude larger than for second neighbors and beyond.

Finally, we also study the effects of anharmonicity by applying first-order perturbation theory to the finite differences results. The total energy versus displacement curve in the harmonic approximation is written as an oscillator potential energy:

$$V_0 = \frac{1}{2m}\omega_{0,shear}^2(x^2 + y^2) + \frac{1}{2m}\omega_{0,LBM}^2 z^2, \tag{8}$$

which is the potential energy of a 3D anisotropic quantum harmonic oscilator whose eigenvectors are $|n_x, n_y, n_z\rangle$ and eigenvalues are $E^{(0)}(n_x, n_y, n_z) = \hbar\omega_{0,shear}(n_x + n_y + 1) + \hbar\omega_{0,LBM}(n_z + 1/2)$. The perturbation potential is given by

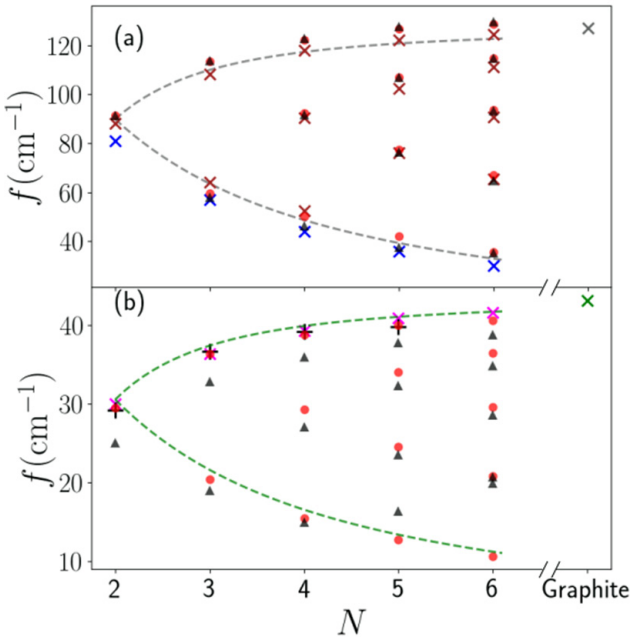

Figure 4. Layer breathing (a) and shear (b) mode frequencies of NLG and graphite at the Γ point. Red dots are calculations using the vdW-DF1-optB88 functional and black triangles are calculations including first order perturbation theory (see text). Experimental values given in [17] (blue crosses), [16] (pink crosses), [20] (black plus signs), [15] (gray crosses) and [18] (brown crosses). Dashed lines are predictions using the experimental values of graphite and equation (7) for the upper and lower branches.

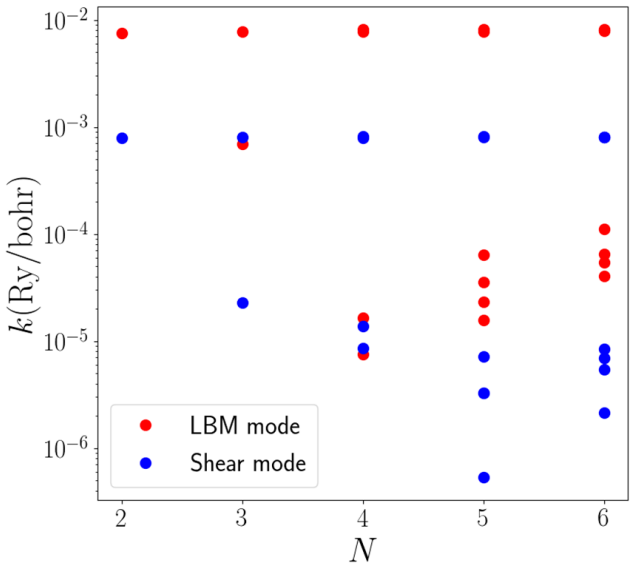

Figure 5. Calculated force constants for NLG given by vdW-DF1-optB88 functional. Red circles correspond to the LBM and blue circles to shear modes.

$$V' = Ax^4 + By^4 + Cz^4. \tag{9}$$

Note that terms of third order on the position operators give a zero contribution to the first order correction. The corrections to the frequencies are $\Delta\omega = \Delta E^{(1)}/\hbar$, where $E^{(1)}(n_x, n_y, n_z) = \langle n_x, n_y, n_z|V'|n_x, n_y, n_z\rangle$ are the first order corrections given by

$$\begin{aligned} &E^{(1)}(n_x, n_y, n_z) \\ &= \left(\frac{\hbar}{2m\omega_{0,\mathrm{shear}}}\right)^2 \left(3A\left(n_x^2 + n_x + \frac{1}{2}\right) + 3B\left(n_y^2 + n_y + \frac{1}{2}\right)\right) \\ &+ \left(\frac{\hbar}{2m\omega_{0,\mathrm{LBM}}}\right)^2 6C\left(n_z^2 + n_z + \frac{1}{2}\right). \end{aligned} \tag{10}$$

For the LBM, the corrections are about a few cm^{-1} and, for the lowest branch in figure 4 they yield a better agreement with data from [17]. For the shear mode, the corrections are larger than for the LBM, but they lead to a worse agreement with experimental results.

4. Conclusions

We have evaluated the performance of different vdW functionals on the description of structural, mechanical and vibrational properties of graphite. Our results indicate that, although the vdW-DF2B86r functional has the best overall performance, the vdW-DF1-optB88 is more adequate for vibrational properties. Many other functionals, such as vdW-DF1-opt86b, vdW-DF-cx and RVV10, show very good agreement with experimental results as well. Even LDA performs well for a few structural properties, but it provides too small exfoliation energies.

To study the vibrational properties of NLG, we used the vdW-DF1-optB88 functional. Calculated vibrational frequencies match with great accuracy available experimental results and predictions of analytical models based on nearest-neighbor layer interactions. This suggests that our methodology has predictive power for the frequencies which have not been measured so far. Our results reinforce the adequacy of recently developed vdW functionals and their importance to the study of graphene-based layered systems, other layered 2D materials and van-der-Waals heterostructures and illustrate the need of inclusion of vdW interactions in order to correctly describe these properties, especially those related to out-of-plane atomic displacements.

Acknowledgments

We acknowledge the financial support from the Brazilian agencies CNPq, CAPES, FAPERJ and INCT-Nanomateriais de Carbono. We also thank DIMAT-Inmetro and COPPE-UFRJ for the computational resources employed on this work.

ORCID iDs

Rafael R Del Grande https://orcid.org/0000-0003-1776-5731
Marcos G Menezes https://orcid.org/0000-0001-8143-0181
Rodrigo B Capaz https://orcid.org/0000-0001-5770-5026

References

[1] Novoselov K S, Geim A K, Morozov S V, Jiang D, Zhang Y, Dubonos S V, Grigorieva I V and Firsov A A 2004 Electric field effect in atomically thin carbon films *Science* **306** 666–9

[2] Novoselov K S, Geim A K, Morozov S V, Jiang D, Katsnelson M I, Grigorieva I V, Dubonos S V and Firsov A A 2005 Two-dimensional gas of massless Dirac fermions in graphene *Nature* **438** 197–200

[3] Geim A K and Novoselov K S 2007 The rise of graphene *Nat. Mater.* **6** 183–91

[4] Geim A K 2009 Graphene: status and prospects *Science* **324** 1530–4

[5] Novoselov K S 2011 Nobel Lecture: graphene: materials in the Flatland *Rev. Mod. Phys.* **83** 837

[6] Castro Neto A H, Guinea F, Peres N M R, Novoselov K S and Geim A K 2009 The electronic properties of graphene *Rev. Mod. Phys.* **81** 109–62

[7] Novoselov K S, Mishchenko A, Carvalho A and Castro Neto A H 2016 2D materials and van der Waals heterostructures *Science* **353** aac9439

[8] Ferrari A C *et al* 2015 Science and technology roadmap for graphene, related two-dimensional crystals, and hybrid systems *Nanoscale* **7** 4598–810

[9] Butler S Z *et al* 2013 Progress, challenges, and opportunities in two-dimensional materials beyond graphene *ACS Nano* **7** 2898–926

[10] Geim A K and Grigorieva I V 2013 Van der Waals heterostructures **499** 419–25

[11] Menezes M G, Capaz R B and Louie S G 2014 *Ab initio* quasiparticle band structure of ABA and ABC-stacked graphene trilayers *Phys. Rev.* B **89** 035431

[12] Vela A, Moutinho M V, Culchac F J, Venezuela P and Capaz R B 2018 Electronic structure and optical properties of twisted multilayer graphene *Phys. Rev.* B **98** 155135

[13] Fang S, Watanabe K, Taniguchi T, Kaxiras E, Cao Y, Fatemi V and Jarillo-Herrero P 2018 Unconventional superconductivity in magic-angle graphene superlattices *Nature* **556** 43–50

[14] Meunier V, Souza Filho A G, Barros E B and Dresselhaus M S 2016 Physical properties of low-dimensional sp^2-based carbon nanostructures *Rev. Mod. Phys.* **88** 025005

[15] Holden J M, Eklund P C and Jishi R A 1995 Vibrational modes of carbon nanotubes; spectroscopy and theory *Carbon* **33** 959–72

[16] Tan P H *et al* 2012 The shear mode of multilayer graphene *Nat. Mater.* **11** 294–300

[17] Lui C H, Ye Z, Keiser C, Xiao X and He R 2014 Temperature-activated layer-breathing vibrations in few-layer graphene *Nano Lett.* **14** 4615–21

[18] Lui C H and Heinz T F 2013 Measurement of layer breathing mode vibrations in few-layer graphene *Phys. Rev.* B **87** 121404

[19] Ijäs M, Han W, Qiao X, Li X, Jiang D, Ferrari A C, Tan P, Wu J and Xin Z 2014 Resonant raman spectroscopy of twisted multilayer graphene *Nat. Commun.* **5** 5309

[20] Boschetto D, Malard L, Lui C H, Mak K F, Li Z, Yan H and Heinz T F 2013 Real-time observation of interlayer vibrations in bilayer and few-layer graphene *Nano Lett.* **13** 4620–3

[21] Lin M-L, Wu J-B, Liu X-L and Tan P-H 2018 Probing the shear and layer breathing modes in multilayer graphene by raman spectroscopy *J. Raman Spectrosc.* **49** 19–30

[22] Berland K, Cooper V R, Lee K, Schröder E, Thonhauser T, Hyldgaard P and Lundqvist B I 2015 Van der Waals forces in density functional theory: a review of the VDW-DF method *Rep. Prog. Phys.* **78** 066501

[23] Langreth D C, Dion M, Rydberg H, Schröder E, Hyldgaard P and Lundqvist B I 2005 Van der waals density functional theory with applications *Int. J. Quantum Chem.* **101** 599–610

[24] Mounet N and Marzari N 2005 First-principles determination of the structural, vibrational and thermodynamic properties of diamond, graphite, and derivatives *Phys. Rev.* B **71** 205214

[25] Dion M, Rydberg H, Schröder E, Langreth D C and Lundqvist B I 2004 Van der waals density functional for general geometries *Phys. Rev. Lett.* **92** 246401

[26] Thonhauser T, Zuluaga S, Arter C A, Berland K, Schröder E and Hyldgaard P 2015 Spin signature of nonlocal correlation binding in metal-organic frameworks *Phys. Rev. Lett.* **115** 136402

[27] Lee K, Murray E D, Kong L, Lundqvist B I and Langreth D C 2010 Higher-accuracy van der Waals density functional *Phys. Rev.* B **82** 081101

[28] Klimeš J, Bowler D R and Michaelides A 2010 Chemical accuracy for the van der Waals density functional *J. Phys.: Condens. Matter* **22** 022201

[29] Klimeš J, Bowler D R and Michaelides A 2011 Van der waals density functionals applied to solids *Phys. Rev.* B **83** 195131

[30] Cooper V R 2010 Van der waals density functional: an appropriate exchange functional *Phys. Rev.* B **81** 161104

[31] Berland K and Hyldgaard P 2014 Exchange functional that tests the robustness of the plasmon description of the van der Waals density functional *Phys. Rev.* B **89** 035412

[32] Hamada I 2014 Van der Waals density functional made accurate *Phys. Rev.* B **89** 121103

[33] Sabatini R, Gorni T and de Gironcoli S 2013 Nonlocal van der Waals density functional made simple and efficient *Phys. Rev.* B **87** 041108

[34] Schröder E, Cooper V R, Berland K, Lundqvist B I, Hyldgaard P and Thonhauser T 2017 VDW-DF family of nonlocal exchange-correlation functionals *Non-Covalent Interactions in Quantum Chemistry and Physics* (Elsevier: Amsterdam) pp 241–74

[35] Giannozzi P *et al* 2009 Quantum espresso: a modular and open-source software project for quantum simulations of materials *J. Phys.: Condens. Matter* **21** 395502

[36] Giannozzi P *et al* 2017 Advanced capabilities for materials modelling with quantum espresso *J. Phys.: Condens. Matter* **29** 465901

[37] Perdew J P, Burke K and Ernzerhof M 1996 Generalized gradient approximation made simple *Phys. Rev. Lett.* **77** 3865–8

[38] Perdew J P and Zunger A 1981 Self-interaction correction to density-functional approximations for many-electron systems *Phys. Rev.* B **23** 5048–79

[39] Rappe A M, Rabe K M, Kaxiras E and Joannopoulos J D 1990 Optimized pseudopotentials *Phys. Rev.* B **41** 1227–30

[40] Boettger J C 1997 All-electron full-potential calculation of the electronic band structure, elastic constants, and equation of state for graphite *Phys. Rev.* B **55** 11202–11

[41] Björkman T, Gulans A, Krasheninnikov A V and Nieminen R M 2012 Van der Waals bonding in layered compounds from advanced density-functional first-principles calculations *Phys. Rev. Lett.* **108** 1–5

[42] Han M, Beister H and Syassen K 1989 Graphite under pressure: equation of state and first-order raman modes *Phys. Rev.* B **39** 12598–603

[43] Rand B 2000 Graphite and Precursors ed P Delhaes (Boca Raton, FL: CRC Press) ch 6 pp 111–40

[44] Bosak A, Krisch M, Mohr M, Maultzsch J and Thomsen C 2007 Elasticity of singlecrystalline graphite: inelastic x-ray scattering study *Phys. Rev.* B **75** 153408

[45] Zacharia R, Ulbricht H and Hertel T 2004 Interlayer cohesive energy of graphite from thermal desorption of polyaromatic hydrocarbons *Phys. Rev.* B **69** 155406

[46] Liu Z, Liu J Z, Cheng Y, Li Z, Wang L and Zheng Q 2012 Interlayer binding energy of graphite: a mesoscopic determination from deformation *Phys. Rev.* B **85** 205418
[47] Benedict L X, Chopra N G, Cohen M L, Zettl A, Louie S G and Crespi V H 1998 Microscopic determination of the interlayer binding energy in graphite *Chem. Phys. Lett.* **286** 490–6
[48] Wang W, Dai S, Li X, Yang J, Srolovitz D J and Zheng Q 2015 Measurement of the cleavage energy of graphite *Nat. Commun.* **6** 1–7
[49] Rêgo C R, Oliveira L N, Tereshchuk P and Da Silva J L 2015 Comparative study of van der Waals corrections to the bulk properties of graphite *J. Phys.: Condens. Matter* **27** 415502
[50] Lebègue S, Harl J, Gould T, Ángyán J G, Kresse G and Dobson J F 2010 Cohesive properties and asymptotics of the dispersion interaction in graphite by the random phase approximation *Phys. Rev. Lett.* **105** 196401
[51] Spanu L, Sorella S and Galli G 2009 Nature and strength of interlayer binding in graphite *Phys. Rev. Lett.* **103** 196401
[52] Chen X, Tian F, Persson C, Duan W and Chen N X 2013 Interlayer interactions in graphites *Sci. Rep.* **3** 3046
[53] Kunc K and Martin R M 1982 *Ab initio* force constants of gaas: a new approach to calculation of phonons and dielectric properties *Phys. Rev. Lett.* **48** 406–9
[54] Alzyab B, Perry C H, Zahopoulos C, Pringle O A and Nicklow R M 1988 High-pressure neutron-scattering studies of graphite and stage-two graphite-SBCL5 *Phys. Rev.* B **38** 1544–7
[55] Brown L, Hovden R, Huang P, Wojcik M, Muller D A and Park J 2012 Twinning and twisting of tri- and bilayer graphene *Nano Lett.* **12** 1609–15